Absorption and Fluorescence Excitation Spectra of 9-(*N*-carbazolyl)-anthracene: Effects of Intramolecular Vibrational Redistribution and Diabatic Transitions Involving Electron Transfer†

F. Evers,‡ J. Giraud-Girard,§ S. Grimme,|| J. Manz,*,⊥ C. Monte,# M. Oppel,⊥ W. Rettig,# P. Saalfrank,▽ and P. Zimmermann‡

Institut für Atomare und Analytische Physik, Technische Universität Berlin, Hardenbergstrasse 36, 10623 Berlin, Germany, Laboratoire de Chimie Quantique, CNRS URA 505, IRSAMC, Université Paul Sabatier, 118 route de Narbonne, 31062 Toulouse Cedex, France, Organisch-Chemisches Institut der Westfälischen Wilhelms-Universität Münster, Corrensstrasse 40, 48149 Münster, Germany, Institut für Chemie—Physikalische und Theoretische Chemie, Freie Universität Berlin, Takustrasse 3, 14195 Berlin, Germany, Institut für Chemie der Humboldt Universität Berlin, Physikalische und Theoretische Chemie, Bunsenstrasse 1, 10117 Berlin, Germany, and Institut für Physikalische und Theoretische Chemie, Universität Regensburg, Universitätsstrasse 31, 93053 Regensburg, Germany

Received: October 20, 2000

The absorption and fluorescence excitation spectra of 9-(*N*-carbazolyl)-anthracene (C9A) in vibronically excited S_1 states are measured and calculated by means of a simple model. Accordingly, C9A is excited from torsional states $|0j\rangle$ of the electronic ground-state S_0 to diabatic torsional states $|1l\rangle$ of the bright electronically excited state S_1, which are coupled to states $|2l\rangle$ of the dark electronically excited-state S_2. In addition, all torsional states are coupled to the other vibrations of C9A. The model parameters are adapted from our previous papers yielding good agreement of the experimental and theoretical fluorescence emission spectrum and fluorescence lifetimes of C9A. The present additional agreement for the experimental and theoretical absorption and fluorescence excitation spectra confirms the simple model, which implies rather weak couplings of the torsional bright state S_1 but strong coupling of the dark state S_2 to the other vibrations of C9A, respectively. This points to different electronic structures of these excited states. This conjecture is confirmed by quantum chemical calculations based on density functional theory (DFT) that reveal the covalent structure of S_1, in contrast with the TICT (twisted intramolecular charge transfer) behavior of S_2.

I. Introduction

Electron transfer (ET) is one of the most important photochemical primary processes, not only because it is at the basis of earth's life through photosynthesis but also because theories have been developed that are able to quantify its energetics and its kinetics. A breakthrough in this respect was the Marcus theory,[1,2] which has engendered an enormous number of scientific publications, mainly on so-called weakly coupled electron-transfer systems.[3] In parallel, a different branch of electron transfer has been developed experimentally, that of the so-called "twisted intramolecular charge transfer" (TICT) states, which often involve two strongly coupled near-planar π-systems linked by a flexible single bond (for reviews, see refs 4−7). The interesting and astonishing fact about TICT states is their "minimum overlap" behavior connected with a twisted geometry, resulting in a weak coupling between the π-subunits. Photoinduced electron transfer occurs somewhere along the reaction path leading from the primarily excited strongly coupled excited state to the weakly coupled TICT state. Therefore, in general, TICT-type electron transfer reactions cannot be considered to be situated in the Marcus weak-coupling limit. Nevertheless, considerable advances have been made recently by the application of the Marcus theory[8] to the emission spectra of TICT-type large biaryls.[9−14]

9,9′-Bianthryl (BA) is the prototype TICT-type large biaryl and has been studied extensively since the discovery of its dual fluorescence in polar solvents.[15] The normal fluorescence band corresponds to the anthracene-type state, delocalized over the two halves (DE = delocalized excited state); it is also often called the locally excited (LE) state. The second fluorescence band is identified as charge-transfer band from its solvatochromic red shift[15−17] and corresponds to a solvent-polarity-induced charge separation creating a symmetry-broken pair of anthracene cation−anion radicals. This has been demonstrated by transient absorption measurements.[18] Carbazole is isoelectronic with anthracene, and therefore anthrylcarbazoles can be compared directly to the corresponding bianthryls. As carbazole is a better electron donor than is anthracene, the carbazole derivative corresponding to 9,9′-bianthryl, 9-(*N*-carbazolyl)anthracene (C9A) exhibits an increased tendency for charge transfer (CT) formation, which should lead to a decreased weight of the "delocalized" excited state (DE) in the excited-state equilibrium between DE and CT.[16,18] We shall adapt the notation "DE" for the emissive excited state of C9A cooled in the jet, by analogy with BA which serves as a reference, irrespective of a much smaller "delocalization" in C9A, in comparison with BA, see section IV below. The model system C9A is illustrated in Figure

† Part of the special issue "William H. Miller Festschrift".
‡ Technische Universität Berlin.
§ Université Paul Sabatier.
|| Westfälischen Wilhelms-Universität Münster.
⊥ Freie Universität Berlin.
Humboldt Universität Berlin.
▽ Universität Regensburg

10.1021/jp003879d CCC: $20.00
Published on Web 03/22/2001

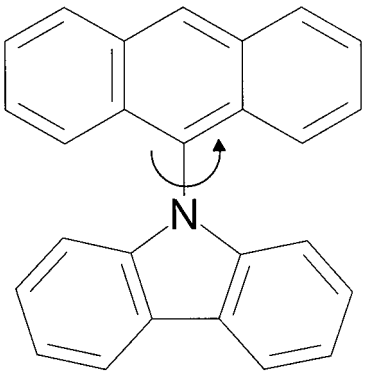

Figure 1. 9-(*N*-Carbazolyl)-anthracene C9A. Torsion around the central CN bond is indicated by the arrow. The torsional angle $\theta = 90$ corresponds to the perpendicular configuration of the carbazolyl and anthracene moieties.

1. Both BA and C9A show ultrafast formation of the CT state in solution in the picosecond range.[19−23] Gas-phase supersonic jet studies are also available for C9A,[24] which have revealed a tremendous amount of detailed information and have uncovered an outstanding example of a photoreaction with resonance behavior, i.e., the reaction occurs just in the vicinity of a certain excitation energy. A further rise of the excitation energy leads to a slowing-down of the reaction. This is contrary to the usual Arrhenius-type barrier behavior in which increasing thermal energy always leads to an acceleration of the reaction. There are strong arguments suggesting that this reaction corresponds to the charge-transfer reaction seen in solution. Both BA, its cyano derivative BACN and C9A have been studied under jet conditions,[24,25] and the gas phase twist potentials of S_0 and S_1(DE) can be determined accurately from fluorescence excitation and dispersed fluorescence spectra as a function of excess energy, even if the 0−0 band is not observable. Accordingly, the minima of the ground state double-minimum potential of C9A are shifted with respect to the excited state minima and are situated below a steeply rising potential region of S_1 (DE),[24] see Figure 2, adapted from ref 26. Therefore, many levels of the S_1 torsional vibration can be excited optically. This leads to a very rich fluorescence excitation spectrum, consisting of a multitude of lines spaced by approximately 37 cm^{-1} with an unobservable 0−0 transition. From the detailed knowledge of S_0 and S_1 potentials, the Franck−Condon factors (intensity distribution) can be calculated accurately and compared to the experiment. Most remarkably, the envelope of the spectrum presents a pronounced minimum of the intensity, which is not explainable from the potential shape. It is, however, understandable if a process competing with fluorescence leads to fluorescence quenching at this excess energy (ca. 470 cm^{-1}). This assumption could be verified by measuring separately the fluorescence lifetimes, which also show a pronounced shortening at this excess energy, corresponding to a photoprocess that is fastest at this excess energy but slows down if the energy is larger or smaller (the resonance behavior introduced above).

Interestingly, this shortening (ns range) is 3 orders of magnitude slower in the gas phase than in solution (ps formation of the CT state). The photoprocess has been interpreted as crossing of the emissive state S_1(DE) with a nonemissive "dark" state S_X, with probable charge transfer nature possessing a potential minimum at considerably different twist angles. The present contribution brings additional arguments for this assignment. In particular, we shall demonstrate and anticipate the adequate notation that the formally unknown state S_X is indeed the second excited electronic state S_2 at 70°. This terminology is adapted from the diabatic potentials, independent of the torsional angle. A third independent confirmation of this resonance-type photoprocess can be gained by measuring the absorption spectrum for jet conditions with the cavity-ring-down method, which is described in the present contribution. At this point, theoretical modeling can be very helpful to unravel additional details of the ongoing photoprocess. The twist dynamics of C9A has been modeled on the femtosecond/picosecond time scale based on the time-dependent density matrix formalism, and the spectra have been calculated therefrom and compared to experiment.[26−29] These studies show that the assumption of a dark state S_2 with a potential minimum at $\theta = 90°$, as shown in Figure 2, is a reasonable approach that satisfactorily reproduces the observed fluorescence lifetimes. Moreover, these model calculations even allow to estimate the relative energy of the minima of S_1 and S_2. If the excess excitation energy is too small to reach the crossing of the two states S_1(DE) with S_2(CT) at the critical energy E_c, the wave packet generated oscillates rather undisturbed i.e., coherently around the minima of S_1(DE), with a characteristic torsional period of about 1 ps. For excitation energies that reach the crossing exactly, efficient transfer of the population to S_2 occurs, which is, however, transferred back from S_2 to S_1 nearly completely after half an oscillation period. Some of this population can, however, remain trapped in S_2 and accumulate there if dissipative processes such as intramolecular vibrational redistribution (IVR) from the torsional to the vibrational modes are faster in this state than in S_1. More efficient IVR in S_2 than in S_1 points to stronger coupling of the torsional and background vibrations in S_2 than in S_1, and this could be a consequence of the CT nature of the S_2 state, in comparison with the non-CT nature of S_1(DE). As a result, rapid IVR in S_2 induces energy relaxation down to the lower levels of the torsional motion within S_2, which are coupled to accepting modes playing the role of a thermal heat bath introducing irreversibility. The shortening of the fluorescence decay time in the nanosecond range in this model corresponds to the irreversible trapping of the population in S_2 by IVR. These calculations reveal a nearly coherent torsional motion of C9A(S_1) on the time scale of ca. 1 ps to 100 ps and longer,[27,29] which is quite surprising for a large organic molecule such as C9A(S_1), implying that IVR for this torsional mode is on a very slow (nanosecond) time scale. This is presumably a consequence of the rather weak coupling of the torsional motion to the other vibrations. This detailed picture of ET, which is possible due to the high resolution of the jet experiment and the combination with wave packet calculations, thus shows that (i) the CT state is confined to more strongly twisted geometries than the DE state and (ii) the actual electron-transfer step occurs in the gas phase at a specific geometry and can be treated as a nonadiabatic surface crossing process in this case.

The present contribution adds new experimental results (absorption under jet conditions) and combines them with high-level quantum-chemical calculations within a density functional theory (DFT) and multireference configuration interaction (MRCI) approach for excited states[30] and with a theoretical modeling of the observed absorption and emission spectra thus yielding new information on the $S_X = S_2$ potential, its electronic nature, and the nonadiabatic transition.

II. Experimental Determination of the Absorption Spectrum in the Jet

A. Cavity Ring-Down Spectroscopy. In the past it was very difficult to determine absorption coefficients with sufficient

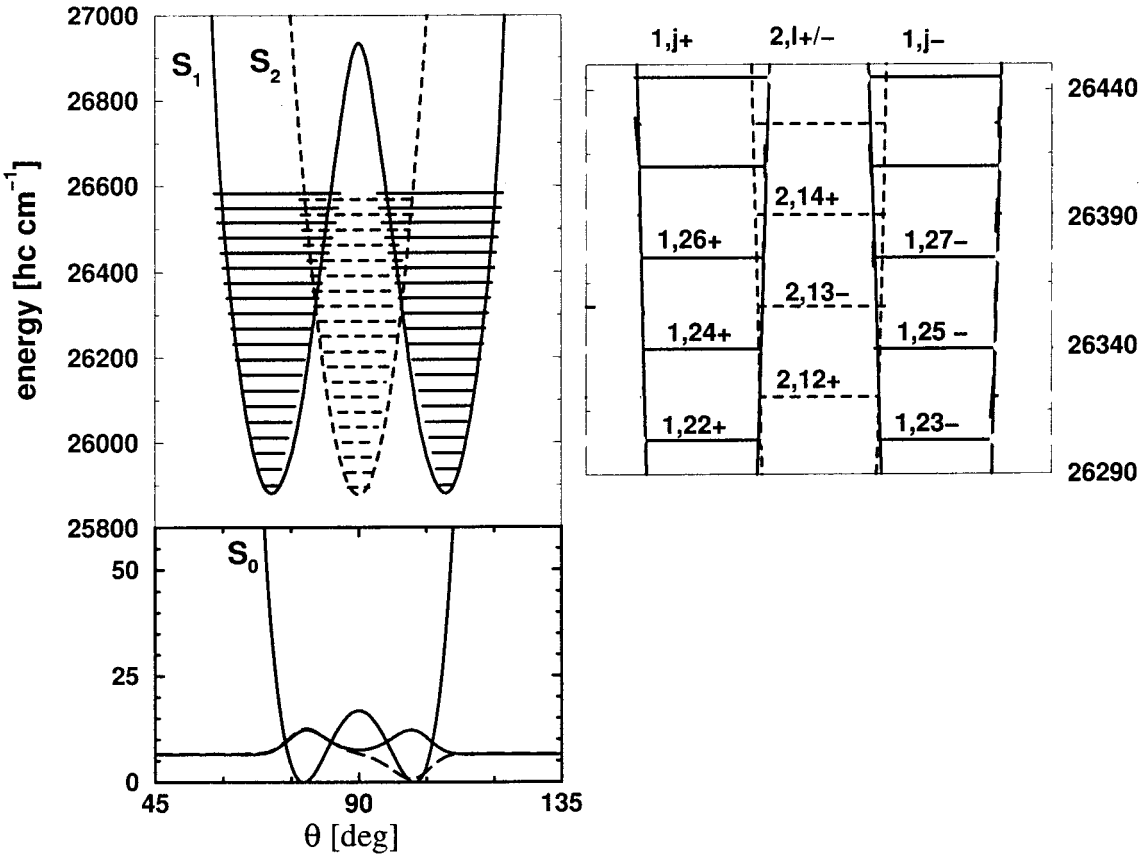

Figure 2. Diabatic potential energy curves V^0, V^1, and V^2 of C9A versus torsional angle θ, together with the diabatic levels E_j^0, E_j^1, and E_j^2 for the delocalized states $|0j\pm\rangle$, $|1j\pm\rangle$ and the localized ones $|2j\rangle$, respectively. Also shown are the delocalized torsional wave functions for the lowest near-degenerate pair of levels, $E_{0,+}^0$ and $E_{1,-}^0$ with + and − parity, respectively. The right panel shows a blow-up of the left panel in the region of the crossing of the V^1 and V^2 (adapted from ref 26).

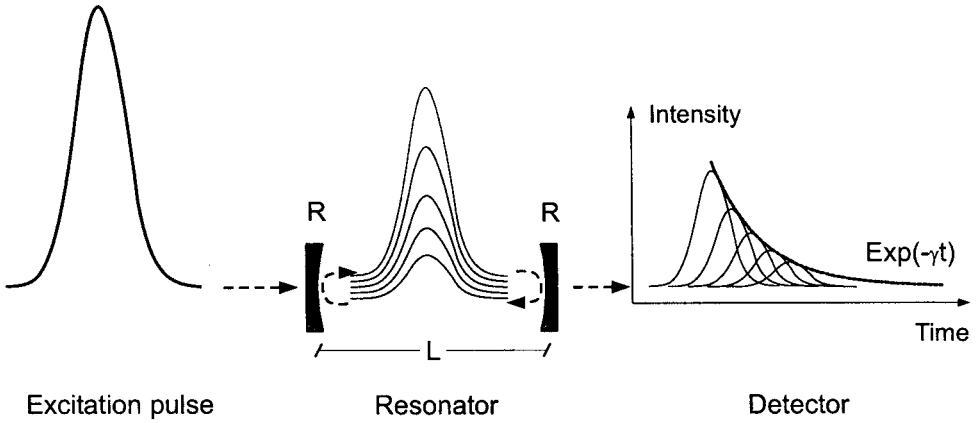

Figure 3. Schematic representation of a cavity ring-down experiment (see text).

accuracy in a free molecular beam due to its extremely weak density. Complex experimental methods such as laser intracavity spectroscopy for example were necessary to get the desired information.

A new sensitive method was developed[31] which allows the measurement of absorption coefficients in very dilute gaseous media using a relatively simple setup: the cavity ring-down spectroscopy. The sensitivity is high enough to allow the determination of absorption coefficients even in molecular beams.[32] The emerging field of cavity ring-down spectroscopy has recently been reviewed in ref 33. For further reading see also refs 34 and 35.

In the following, the principle of cavity ring-down spectroscopy will be discussed briefly for the general reader. The central element of the setup is an optical cavity with highly reflective mirrors (typical $R = 0.997$ or better) on both sides. A laser pulse enters this cavity from one direction. Due to the high reflectivity R, only a small fraction $(1 - R)$ of the laser pulse is coupled into the cavity.

After passing the cavity in one direction, an even smaller part $(1 - R)^2$ of the laser beam is coupled out through the second mirror. The fraction $(1 - R) - (1 - R)^2$ remains inside the cavity. After the next roundtrip, which is complete after the time T, the quantity $((1 - R) - (1 - R)^2)\cdot(1 - R)^2)$ is coupled out. After many roundtrips, a series of pulses with approximately exponentially decreasing intensity is obtained (Figure 3). The light that is coupled out of the cavity is detected by a fast and

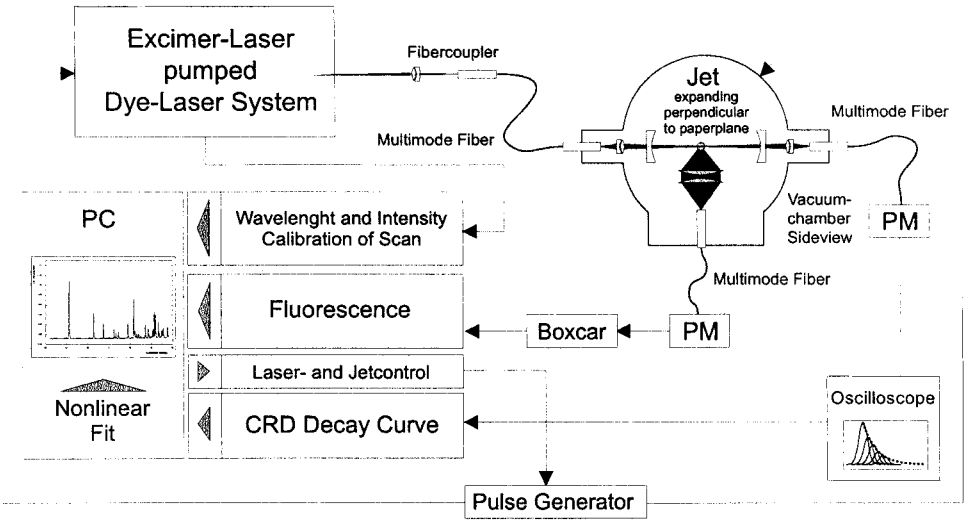

Figure 4. The experimental setup for cavity ring-down and fluorescence excitation spectroscopy. A personal computer controls a pulsed excimer pumped dye-laser system and the pulsed molecular beam. The laser light is coupled through an optical multimode fiber into the cavity ring-down resonator. The cavity ring-down signal is detected through a multimode fiber on a microchannel plate and processed on a storage oscilloscope. The obtained decay curve is transferred to the personal computer. A nonlinear fit delivers the relative absorption. The total fluorescence is detected perpendicular to the cavity ring-down resonator. The light passes through a multimode fiber to a photomultiplier. The photomultiplier signal is processed by a boxcar integrator and delivered to the personal computer as relative fluorescence excitation. By scanning the dye laser, an absorption and an excitation spectrum could be recorded simultaneously.

sensitive detector. The series of pulses results in a decreasing intensity curve that can be fitted exponentially (compare Figure 3).

The exponential decay constant depends on the reflectivity of the mirrors. A higher reflectivity leads to a longer decay. An absorbing species in the cavity can be viewed as a higher loss or a smaller reflectivity R, which results in a faster decay (larger decay constant γ in Figure 3). By tuning the excitation source across a wavelength interval and recording the decay constants it is thus possible to record an absorption spectrum.

Our experimental setup is shown in Figure 4. The setup used here has several advantages: The main advantage is that fluorescence excitation and absorption spectra can be recorded simultanously. Hence, it is possible to detect directly the losses in the fluorescence quantum yield (i.e., "dark" photoreactions) by comparing the two spectra.

An experimental advantage of our setup is that the adjustment of the cavity with respect to the laser and the simultaneous adjustment of the fluorescence detection area are simplified by using optical fibers. A single adjustment of the optical system within the vacuum chamber is usually sufficient. At later times, it is necessary to adjust the laser only with respect to the fiber coupler. All sensitive components remain fixed. The laser system and the experimental details of the setup are described in more detail in ref 36.

B. Results. Figure 5 shows the recorded cavity ring-down (CRD) spectrum in the vicinity of the resonant photoreaction of C9A, i.e., near the depression in the Franck−Condon profile of the fluorescence excitation spectrum.[37] The CRD spectrum is compared with the simultanously recorded fluorescence excitation spectrum. The difference of the intensity pattern of the main progression (lines: 26296, 26331, 26366, 26401, and 26436 cm^{-1}) in both spectra is obvious. There is a relative decrease of the intensity for the lines at 26331 and 26366 cm^{-1} in both the fluorescence excitation and the absorption spectrum, but this decrease is significantly stronger in the excitation spectrum than in the absorption spectrum. This is an indication for internal conversion (IC) from the "bright" excited state (S_1) to the "dark" resonant state (S_2), at that excitation energy. Further details of the experimental spectra are discussed in ref 36.

The labeled bands in the recorded spectra in Figure 5 are fitted with the same line profile. The derived relative intensity values for the cavity ring-down spectrum are given in Table 1.

III. Quantum Dynamics and Spectroscopy

In the following, the theoretical approach to the dissipative dynamics and the spectroscopy of the C9A molecule are outlined. Because details of the quantum dynamical model and details of how to evaluate IVR rates and fluorescence lifetimes have been published elsewhere,[26,29] the corresponding parts of this theory section will be kept in brief.

A. Model Hamiltonian. In the following, the entire (but still isolated) C9A molecule will be described by the Hamiltonian

$$\hat{H} = \hat{H}_{\mathrm{tor}} + \hat{H}_{\mathrm{vib}} + \hat{H}_{\mathrm{tor-vib}} \tag{1}$$

Here, $\hat{H}_{\mathrm{tor}}$ is the *torsional* Hamiltonian accounting for the torsion of the two moieties of C9A around the central C−N bond. $\hat{H}_{\mathrm{vib}}$ models those vibrational degrees of freedom of the molecule which are not included in $\hat{H}_{\mathrm{tor}}$. We idealize them as a set of harmonic oscillators (see below). Finally, $\hat{H}_{\mathrm{tor-vib}}$ gives the coupling between the twist and these bath modes.

Considering three *diabatic* electronic states S_0 (ground state), S_1 (bright excited state), and S_2 (dark excited state), we have for the torsional Hamiltonian

$$\hat{H}_{\mathrm{tor}} = \hat{H}^{00}_{\mathrm{tor}}|0\rangle\langle 0| + \hat{H}^{11}_{\mathrm{tor}}|1\rangle\langle 1| + \hat{H}^{22}_{\mathrm{tor}}|2\rangle\langle 2| + (\hat{H}^{01}_{\mathrm{tor}}|0\rangle\langle 1| + \mathrm{h.c.}) + (\hat{H}^{12}_{\mathrm{tor}}|1\rangle\langle 2| + \mathrm{hc}) \tag{2}$$

where h.c. denotes the hermitian conjugate and where it is assumed that the S_0 state is dipole coupled only to S_1, whereas S_1 is dipole coupled to S_0 and adiabatically coupled to S_2 (see below). Note that the dark state S_2 has been labeled as state 'X' in ref 26, thus indicating its unknown electronic nature. Here we anticipate the present new results of the quantum

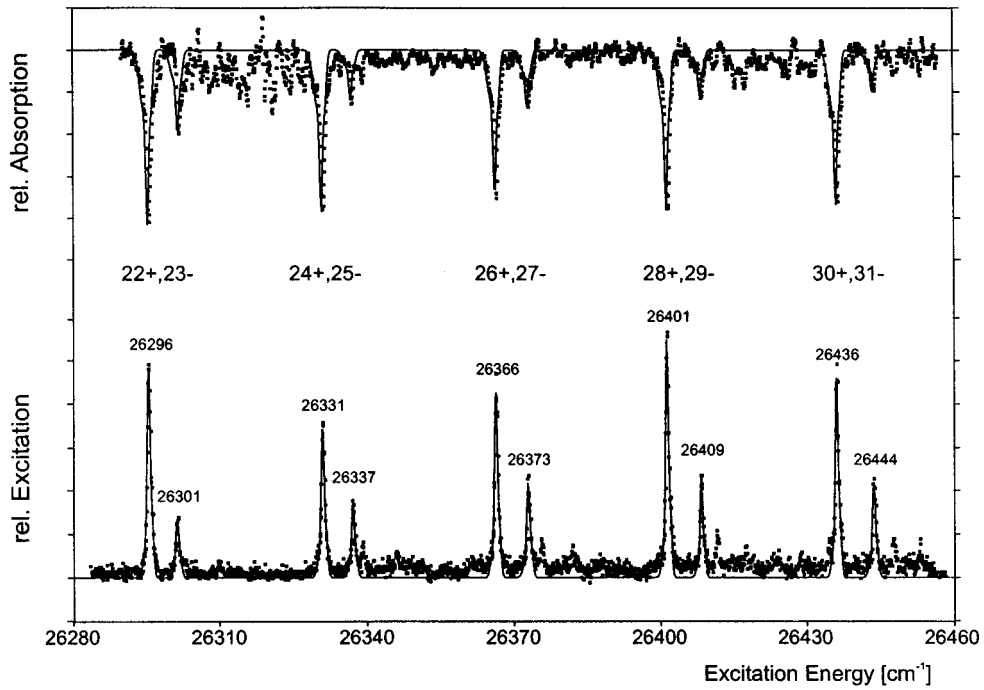

Figure 5. The recorded cavity ring-down spectrum in the upper half is compared with the simultanously recorded fluorescence excitation spectrum in the lower half. The recorded signals are shown as dots. The fitted line shapes are shown as continuous line. Relative intensity values are shown. The lines of the main progression are labeled with torsional numbers as well as excitation energies. The lines of a combination progression with lower overall intensity are labeled just by their excitation energy.

TABLE 1: Relative Absorption Intensity Obtained by Cavity Ring-Down Spectroscopy of the C9A Torsional Spectrum[a]

torsional state	excitation energy [cm^{-1}]	rel. absorption intensity	rel. error [%]
22+,23−	26296	0.8777	4.7
24+,25−	26331	0.8187	5.1
26+,27−	26366	0.7191	5.8
28+,29−	26401	0.7767	5.3
30+,31−	26436	0.7719	5.4

[a] The values are given for selected lines of the main progression as indicated in Figure 5. The given errors result from a confidence interval of 90%.

chemical calculations, to be presented below in section IV: they reveal that state 'X' is the second excited electronic singlet state, S_2.

For the diagonal terms in eq 2 we write

$$\hat{H}^{ee}_{tor} = -\frac{\hbar^2}{2I}\frac{\partial^2}{\partial\phi^2} + V^e(\phi) \qquad e = 0, 1, 2 \tag{3}$$

Here, $\phi = \theta - {}^{\pi}/_{2} \in [-\pi/2, \pi/2]$ is the torsional angle in the one-dimensional model, where $\phi = 0$ ($\theta = {}^{\pi}/_{2}$) corresponds to a molecular conformation in which the carbazolyl and anthracene moieties of C9A are oriented perpendicular to each other. I is the corresponding moment of inertia taken from ref 27, which we assume to be identical in all electronic states. Further, $V^e(\phi)$ is the diabatic potential curve corresponding to electronic state $|e\rangle$, for which

$$V^e(\phi) = V^e(-\phi) \tag{4}$$

by symmetry.

For the ground and bright excited states, double minimum potentials of the form

$$V^e(\phi) = -\frac{1}{2}\sum_k^N U^e_{2k}(1 - \cos 2k\phi) \quad e = 0, 1 \tag{5}$$

are used, with parameters taken from ref 24. For the dark state potential we take

$$V^2(\phi) = V_0 + \frac{1}{2}V_2\phi^2 + \frac{1}{24}V_4\phi^4 \tag{6}$$

with potential parameters V_0, V_2, and V_4 adapted from ref 26. V^0 and V^1 exhibit minima at $\pm\phi^0_{min} = 12.5°$ and $\pm\phi^1_{min} = 26°$, respectively, whereas V^2 corresponds to a perpendicular equilibrium structure ($\phi = 0$). These empirical potentials V^0, V^1, and V^2 are shown in Figure 2.

The diabatic torsional eigenstates $|ek\rangle$ of the individual state Hamiltonians $\hat{H}^{ee}_{tor}$,

$$\hat{H}^{ee}_{tor}|ek\rangle = E^e_k|ek\rangle \tag{7}$$

have been calculated previously.[24,26,27] Due to the symmetry restriction imposed by eq 4, the torsional states can be classified according to their parity (+ or −, respectively). Further, the lower states corresponding to the double-minimum potentials V^0 and V^1 form near-degenerate doublets, whereas the quasi-harmonic V^2 potential is characterized by almost equally spaced individual levels.

The *radiative* coupling between the ground-state S_0 and the bright excited-state S_1 is expressed in classical dipole approximation as

$$\hat{H}^{01}_{tor} = \hat{H}^{10}_{tor} = -\hat{\mu}^{01}\cdot\epsilon(t) \tag{8}$$

Here, $\hat{\mu}^{01}$ is the transition dipole moment, which is assumed to be constant under the Condon approximation for the diabatic states, and $\epsilon(t)$ is the (appropriate component of) the external radiation field.

Furthermore, the *nonradiative* coupling between the bright (S_1) and dark (S_2) excited states, describing the adiabatic coupling between them, is assumed to be appropriately represented by two Gaussians centered around the crossing points $\pm\phi_c$, = 13.1° of both potentials:

$$H_{\mathrm{tor}}^{12} = H_{\mathrm{tor}}^{21} = V^{12}(\phi) = C\left(\exp\left\{-\frac{(\phi+\phi_c)^2}{2a^2}\right\} + \exp\left\{-\frac{(\phi-\phi_c)^2}{2a^2}\right\}\right) \quad (9)$$

where the parameters C = 11.0 cm^{-1} and $a = 4.0°$ are taken from ref 26.

The vibrational Hamiltonian $\hat{H}_{\mathrm{vib}}$ occurring in eq 1 provides an intramolecular thermal bath for the torsional motion. It is assumed to be diagonal in the electronic states $|e\rangle$, and it is idealized as a set of uncoupled oscillators in each state:

$$\hat{H}_{\mathrm{vib}} = \sum_{e=0}^{2} \hat{H}_{\mathrm{vib}}^{ee} |e\rangle\langle e| \quad (10)$$

$$\hat{H}_{\mathrm{vib}}^{ee} |v^e\rangle = E_v^e |v^e\rangle \quad (11)$$

Assuming further that (i) electronic transitions do not influence the bath and (ii) that the bath is harmonic, the same F harmonic oscillator states $|v^e\rangle = |v\rangle = |v_1 v_2 \ldots v_F\rangle$ can be adopted for each electronic state, giving

$$E_v^e = E_v = \sum_{m=1}^{F} \hbar\omega_m \left(v_m + \frac{1}{2}\right) = \sum_{m=1}^{F} E_{vm} \quad (12)$$

where ω_m is the harmonic frequency of oscillator m.

For the bath modes, we assume a normalized Ohmic spectral density

$$\rho(\omega_m) = N \cdot \frac{\omega_m}{\omega_c} \cdot \exp\left\{-\frac{\omega_m}{\omega_c}\right\} \quad (13)$$

$$\int_0^\infty \rho(\omega_m)\, d\omega_m = 1 \quad (14)$$

which exhibits a maximum at $\omega_m = \omega_c$. The value $\omega_c = 650$ cm^{-1} is adapted from ref 26.

Finally, for the coupling $\hat{H}_{\mathrm{tor-vib}}$ between the torsional mode and the vibrations, diagonality in the electronic states is assumed as well:

$$\hat{H}_{\mathrm{tor-vib}} = \sum_{e=0}^{2} \hat{H}_{\mathrm{tor-vib}}^{ee} |e\rangle\langle e| \quad (15)$$

The coupling in each state between torsion and intramolecular vibration is taken to be bilinear in the torsional (ϕ) and vibrational (q_m, $m = 1, \ldots F$) modes:

$$\hat{H}_{\mathrm{tor-vib}}^{ee} = \phi \sum_{m=1}^{F} f_m^{(e)} q_m \quad (16)$$

The frequency- and electronic state-dependent coupling constants are assumed to be of the form

$$f_m^{(e)} = f^{(e)} \exp\left\{-\frac{\omega_m}{\omega^{(e)}}\right\} \quad (17)$$

thus emphasizing the preferred coupling of the torsion to low-frequency scaffold oscillators. In the following, we will set $f^{(0)} = 0$, because only the vibrational relaxation in the excited states is of interest here. The remaining model parameters, $f^{(1)} = 1.03$ hc $\mathrm{cm}^{-1}\mathrm{deg}^{-1}$, $f^{(2)} = 103$hc $\mathrm{cm}^{-1}\mathrm{deg}^{-1}$, and $\omega^{(1)} = 80$c cm^{-1}, $\omega^{(2)} = 40c$ cm^{-1} are given in ref 26. It has been emphasized in ref 26 that the coupling strength $f^{(2)}$ in state S_2 is much larger than $f^{(1)}$ in state S_1, but the empirical data allow only a rough estimate of these parameters. The values adapted from ref 26 will also be used in this paper, but other ones yield similar results provided that $f^{(2)}$: $f^{(1)} \geq 10{:}1$.

For the *diabatic* representation above, the coupling between various electronic states can be radiative (coupling between $|0\rangle$ and $|1\rangle$) or nonradiative (coupling between $|1\rangle$ and $|2\rangle$). It turns out to be advantageous in several respects to switch to an adiabatic representation, in which the "excited block" of the field-free, nonradiative Hamiltonian,

$$\hat{H}^E \equiv \sum_{e=1}^{2}\sum_{e'=1}^{2} \hat{H}^{ee'} |e\rangle\langle e'| \quad (18)$$

becomes diagonal, i.e.,

$$\hat{\tilde{H}}^{\hat{E}} = \hat{T}\hat{H}^E\hat{T}^\dagger = \sum_{\tilde{e}=\tilde{1}}^{\tilde{2}} \hat{\tilde{H}}^{\tilde{e}\tilde{e}} |\tilde{e}\rangle\langle\tilde{e}| \quad (19)$$

Accordingly, the new adiabatic basis $\{|\tilde{e}\tilde{k}\rangle\}$ is obtained by numerically diagonalizing the coupled torsional, excited-state system Hamiltonian

$$\hat{H}_{\mathrm{tor}}^E := \hat{H}_{\mathrm{tor}}^{11} |1\rangle\langle 1| + \hat{H}_{\mathrm{tor}}^{22} |2\rangle\langle 2| + (\hat{H}_{\mathrm{tor}}^{12} |1\rangle\langle 2| + \mathrm{hc}) \quad (20)$$

These new excited-state eigenstates $\{|\tilde{e}\tilde{k}\rangle\} \equiv \{|\tilde{1}\tilde{l}\rangle, |\tilde{2}\tilde{m}\rangle\}$ are, due to the "smallness" of the nonradiative coupling operators $\hat{H}_{\mathrm{tor}}^{12}$ and $\hat{H}_{\mathrm{tor}}^{21}$, still very similar to the diabatic basis $\{|1l\rangle, |2m\rangle\}$ with $|1l\rangle$ and $|2m\rangle$ being the eigenstates of $\hat{H}_{\mathrm{tor}}^{11}$ and $\hat{H}_{\mathrm{tor}}^{22}$, respectively; also, the corresponding energy levels $E_{\tilde{k}}^{\tilde{e}}$ and E_k^e are similar. In contrast to the diabatic case, however, the electric field $\epsilon(t)$ now couples the ground-state levels $|0k\rangle$, to all the $N_1 + N_2 = N_{\tilde{1}} + N_{\tilde{2}}$ states of the excited-state manifold. In practice, $N_0 = 2$, $N_1 = 64$, $N_2 = 36$ eigenfunctions have been used as a basis, and the results are converged with respect to N_1 and N_2. The three-state problem with one radiative and one nonradiative interstate coupling has thus been transformed to an effective two-state problem wherein ground state levels $|0k\rangle$ are radiatively coupled only to the excited-state levels $|\tilde{e}\tilde{k}\rangle$. The nonadiabatic couplings for internal conversion are "hidden" in the modified excited-state levels, and their modified coupling to the ground state.

B. Open-System Density Matrix Dynamics. The stationary absorption spectrum for C9A in the presence of IVR and adiabatic couplings between the excited bright and dark states is derived from a time-dependent open-system density matrix approach. Therefore, a brief review of the open-system density matrix approach to the dynamics of C9A is in order: more details can be found in refs 28 and 29. This approach is, in part, also the basis for the derivation of the fluorescence excitation spectrum, see below, and also for the fluorescence lifetimes, see ref 26.

The physical situation we wish to describe below is the following. A photon impulsively excites the C9A molecule, which initially is in its electronic ground state and in thermal equilibrium at (the low) temperature T, to the excited bright state $|1\rangle$. In the diabatic picture, the nonstationary density then

time-evolves in the excited-state manifold under the influence of the coupled, torsional, excited-state system Hamiltonian eq 20. In the adiabatic picture in which the nonradiative excited-state Hamiltonian is diagonal, the impulsive excitation populates all excited states initially with nonvanishing probability, and the subsequent time-evolution proceeds under the influence of

$$\hat{\tilde{H}}^{\tilde{E}}_{\mathrm{tor}} := \hat{\tilde{H}}^{\tilde{1}\tilde{1}}_{\mathrm{tor}}|\tilde{1}\rangle\langle\tilde{1}| + \hat{\tilde{H}}^{\tilde{2}\tilde{2}}_{\mathrm{tor}}|\tilde{2}\rangle\langle\tilde{2}| = T\hat{H}^{E}_{\mathrm{tor}}T^{\dagger} \tag{21}$$

In both pictures, the torsional motion of the excited molecule couples to the intramolecular vibrational environment, leading to IVR of the torsional states. Because the system bath coupling Hamiltonian (eq 15) is assumed to be diagonal in the electronic basis, no environmentally induced electronic relaxation to the ground state takes place. However, on the experimentally known time scale[24] of $\tau_{\mathrm{fl}} \approx 20$ ns, the excited states decay radiatively to S_0 by spontaneous emission (fluorescence).

Apart from the fluorescence decay, the post-excitation dynamics can be described by an open-system Liouville-von Neumann (LvN) equation of the form

$$\mathcal{L}\,\hat{\tilde{\rho}} = \frac{\partial}{\partial t}\hat{\tilde{\rho}} = -\frac{i}{\hbar}[\hat{\tilde{H}}^{\tilde{E}}_{\mathrm{tor}}, \hat{\tilde{\rho}}] + \mathcal{L}_D\hat{\tilde{\rho}} \tag{22}$$

in the adiabatic picture. Here, $\tilde{\rho}$ is the system density operator in the adiabatic basis, and $\mathcal{L}$ and $\mathcal{L}_D$ are the total field-free and dissipative Liouvillian superoperators, respectively. The latter, when acting on $\tilde{\rho}$, describes the time evolution of the density matrix due to environmentally induced relaxation.

In the following, as in previous work,[29] we assume for $\mathcal{L}_D\tilde{\rho}$ the (Markovian) Lindblad semigroup form[38]

$$\mathcal{L}_D\hat{\tilde{\rho}} = \sum_{\tilde{K},\tilde{L}=1}^{N_1+N_2}\Gamma_{\tilde{K}\tilde{L}}\left(\hat{P}_{\tilde{K}\tilde{L}}\hat{\tilde{\rho}}\hat{P}_{\tilde{L}\tilde{K}} - \frac{1}{2}[\hat{P}_{\tilde{L}\tilde{L}},\hat{\tilde{\rho}}]_+\right) \tag{23}$$

which accounts for vibrational energy relaxation and (pure) vibrational dephasing, respectively.[28,39] Here, $\tilde{K} = (\tilde{e}, \tilde{k})$ is a combined electronic/torsional index in the adiabatic representation. Within the adiabatic representation, the operators $\hat{P}_{\tilde{K}\tilde{L}}$ are given by

$$\hat{P}_{\tilde{K}\tilde{L}} = |\tilde{e}\tilde{k}\rangle\langle\tilde{e}'\tilde{l}| \tag{24}$$

In other words, they are ladder operators that connect level $\tilde{l}$ in block $\tilde{e}'$ with level $\tilde{k}$ in block $\tilde{e}$.

Here, $\tilde{e}, \tilde{e}' = \tilde{1}, \tilde{2}$ only because we have set $f^{(0)} = 0$ in eq 17. The use of the adiabatic basis $|\tilde{e}k\rangle$ rather than the diabatic one ($\{|1k\rangle, |2l\rangle\}$) is necessary to provide a well-suited basis for the first-order perturbative treatment to determine the relaxation rate, as discussed elsewhere.[26,29] The $\Gamma_{\tilde{K}\tilde{L}}$ are the corresponding relaxation rates, which shall be specified, for the present model, in the next section.

Equation 22 has been used in ref 29 to elucidate the dissipative quantum dynamics of C9A. Here we will use it as a starting point for the calculation of spectra (see sections below, and the Appendix).

C. IVR Rates. In the present model, finite relaxation rates $\Gamma_{\tilde{K}\tilde{L}}$ for the transitions from states $\tilde{L}$ to $\tilde{K} \neq \tilde{L}$, see eq 23, are a consequence of the coupling of the torsional mode to the not explicitly included molecular vibrations: For the IVR within the adiabatized excited-state manifold, the relevant coupling Hamiltonian assumes the form

$$\hat{\tilde{H}}^{\tilde{E}}_{\mathrm{tor-vib}} = \hat{\tilde{H}}^{\tilde{1}\tilde{1}}_{\mathrm{tor-vib}}|\tilde{1}\rangle\langle\tilde{1}| + \hat{\tilde{H}}^{\tilde{2}\tilde{2}}_{\mathrm{tor-vib}}|\tilde{2}\rangle\langle\tilde{2}| = T(H^{11}_{\mathrm{tor-vib}}|1\rangle\langle 1| + H^{22}_{\mathrm{tor-vib}}|2\rangle\langle 2|)T^{\dagger} \tag{25}$$

where $\hat{H}^{\mathrm{ee}}_{\mathrm{tor-vib}}$ has been defined in (eq 16). Using first-order time-dependent perturbation theory and the coupling (eq 25) in the bilinear form (eq 16) we have derived an expression for the vibrational transition rates $\Gamma_{\tilde{K}\tilde{L}}$ connecting adiabatic torsional levels in the excited-state manifold.[26] Accordingly, the rate for an IVR transition from level $|\tilde{L}\rangle = |\tilde{e}\tilde{l}\rangle$ to $|\tilde{K}\rangle = |\tilde{e}'\tilde{k}\rangle \neq |\tilde{L}\rangle$, at temperature T, is given as

$$\Gamma_{\tilde{K}\tilde{L}}(T) = \frac{2\pi}{\hbar}\rho(\omega_{\tilde{m}})\cdot|\langle\tilde{K}|\hat{T}\phi|1\rangle\langle 1|\hat{T}^{\dagger}|\tilde{L}\rangle f^{(1)}_{\tilde{m}} + \langle\tilde{K}|\hat{T}\phi|2\rangle\langle 2|\hat{T}^{\dagger}|\tilde{L}\rangle f^{(2)}_{\tilde{m}}|^2\cdot\overline{|q_{\tilde{m}}|^2} \tag{26}$$

Here,

$$\overline{|q_{\tilde{m}}|^2} := \frac{1}{2}[(e^{\beta\hbar\omega_{\tilde{m}}} - 1)^{-1} + 1] \tag{27}$$

with $\beta = 1/k_{\mathrm{B}}T$ and k_{B} being Boltzmann's constant, is the Boltzmann average of the squared vibrational transition element for the harmonic bath oscillators, and $\hbar\omega_{\tilde{m}} = E_{\tilde{K}} - E_{\tilde{L}}$ is that bath vibrational quantum, which has to be absorbed/emitted by the system from/to the bath, to account for total energy conservation when the system transition $|\tilde{L}\rangle \rightarrow |\tilde{K}\rangle$ is made. Microsopic reversibility of these vibrational energy transfer processes between the system and the bath yields detailed balance for the rates (eq 26), see ref 26, i.e., a nonequilibrium system will thermalize with the bath held at temperature T in the long-time limit. In the present model, these IVR transition rates $\Gamma_{\tilde{K}\tilde{L}}$ ($\tilde{K} \neq \tilde{L}$) will be used for the Lindblad form of the dissipative time evolution operator eq 23. For the diagonal terms $\Gamma_{\tilde{K}\tilde{K}}$, we shall define[28]

$$\Gamma_{\tilde{K}\tilde{K}} = \sum_{\tilde{L}\neq\tilde{K}}\Gamma_{\tilde{L}\tilde{K}} \tag{28}$$

D. Calculation of Absorption Spectra. As shown by Neugebauer et al.,[40] the linear absorption coefficient $\alpha(\omega)$ for a system in contact with a bath and an external continuous-wave (cw) field, can be obtained from a "generalized Heller formula"[41]

$$\alpha(\omega) = A\omega\cdot\mathrm{Re}\int_0^{\infty} e^{i\omega t}\,\mathrm{tr}\{\hat{\mu}e^{\mathcal{L}t}[\hat{\mu},\hat{\rho}_0]\}\,dt \tag{29}$$

where ω is the light frequency, and A a constant. Furthermore, $\mathcal{L}$ denotes the total Liouvillian, defined in eq 22, $\hat{\mu}$ is the transition dipole operator introduced above, and $\hat{\rho}_0$ is the initial thermal equilibrium density operator of the system. In the diabatic basis, only states $|0\rangle$ and $|1\rangle$ are radiatively coupled, such that

$$\hat{\mu} = \hat{\mu}^{01}|0\rangle\langle 1| + \mathrm{hc} \tag{30}$$

whereas in the adiabatic basis we have

$$\hat{\mu} = \hat{\mu}^{0\tilde{1}}|0\rangle\langle\tilde{1}| + \hat{\mu}^{0\tilde{2}}|0\rangle\langle\tilde{2}| + \mathrm{hc} \tag{31}$$

Treating the two excited states as a single one, $|\tilde{E}\rangle$, we may write the latter equation as

$$\hat{\mu} = \hat{\mu}^{0\tilde{E}}|0\rangle\langle\tilde{E}| + \mathrm{hc} \tag{32}$$

The initial, thermal equilibrium reduced density operator is

$$\hat{\rho}_0 = \frac{e^{-\beta \hat{H}_{tor}}}{Q} \tag{33}$$

with $Q = \mathrm{tr}\{e^{-\beta \hat{H}_{tor}}\}$ being the system partition function. For all practical purposes, the thermal population of electronic excited states can be neglected, such that

$$\hat{\rho}_0 = \mathrm{diag}\left\{\frac{1}{Q}, \frac{e^{-\beta(E_1{}^0 - E_0{}^0)}}{Q}, \frac{e^{-\beta(E_2{}^0 - E_0{}^0)}}{Q}, ...\right\}|0\rangle\langle 0| \tag{34}$$

In other words, only the electronic ground-state torsional levels are populated with Boltzmann weights $p_r^0 = e^{-\beta(E_r{}^0 - E_0{}^0)}/Q$. Note that Q and, therefore $\hat{\rho}_0$, are the same in the adiabatic and diabatic excited-state bases.

Because, in our model, dissipation is of Lindblad form (eq 23), diagonal and off-diagonal elements of the operator $\hat{\sigma}_0 = [\hat{\mu}, \hat{\rho}_0]$ evolve uncoupled under the action of the field-free propagator e^{Lt}, and, as shown in the Appendix, eq 29 can then be evaluated analytically. Let $R = (0, r)$ and $\tilde{K} = (\tilde{E}, \tilde{k})$ be combined indices for the electronic state and torsional level, then the analytical expression for the linear absorption coefficient is, when antiresonances are neglected,

$$\alpha(\omega) = A\omega \sum_R \sum_{\tilde{K}} p_R \cdot |\mu_{R\tilde{K}}|^2 \cdot \frac{\Gamma_{\tilde{K}\tilde{K}}}{(\Gamma_{\tilde{K}\tilde{K}})^2 + (\omega - \omega_{R\tilde{K}})^2} \tag{35}$$

Here, the sums $\sum_R$ and $\sum_{\tilde{K}}$ are over all of the N_0 levels R and the $N_1 + N_2$ levels $\tilde{K}$, respectively, and

$$p_R = p_r^0 \tag{36}$$

$$\mu_{R\tilde{K}} = \langle 0r|\hat{\mu}|\tilde{E}\tilde{k}\rangle \tag{37}$$

$$\omega_{R\tilde{K}} = (E_{\tilde{k}}^{\tilde{E}} - E_r^0)/\hbar \tag{38}$$

The absorption spectrum (eq 35) is thus a sum of broadened Lorentzians. To evaluate the spectrum, we need the Boltzmann weights of the initial (ground) states, eq 36, the transition dipole moments, eq 37, the excitation energies, eq 38, and, finally, the vibrational relaxation rates. If the latter are all zero, eq 35 degenerates to the usual Franck−Condon spectrum of an isolated system. In general, the line width becomes temperature dependent through the transition rates $\Gamma_{\tilde{K}\tilde{K}}$ equation (eq 27). Another source of temperature dependence of the absorption spectrum arises from the Boltzmann weights p_R in eq 35.

Equation 35 for the linear absorption coefficient $\alpha(\omega)$ can readily be extended to more general types of relaxation. One extension is for the case where the excited states $|\tilde{K}\rangle$ do not only decay by IVR with rate

$$\Gamma_{\mathrm{IVR},\tilde{K}} = \Gamma_{\tilde{K}\tilde{K}} \tag{39}$$

but also by radiation, with rate

$$\Gamma_{\mathrm{rad},\tilde{K}} = \hbar/\tau_{\mathrm{rad},\tilde{K}} \tag{40}$$

where $\tau_{\mathrm{rad},\tilde{K}}$ is the radiative lifetime of level $|\tilde{K}\rangle$. The total rate is then

$$\Gamma_{\tilde{K}} = \Gamma_{\mathrm{IVR},\tilde{K}} + \Gamma_{\mathrm{rad},\tilde{K}} \tag{41}$$

and the suggested expression for the linear absorption coefficient $\alpha(\omega)$ is, by analogy with eq 35,

$$\alpha(\omega) = A\omega \sum_{R=1}^{N_0} \sum_{\tilde{K}=1}^{N_1+N_2} p_R \cdot |\mu_{R\tilde{K}}|^2 \cdot \frac{\Gamma_{\tilde{K}}}{(\Gamma_{\tilde{K}})^2 + (\omega - \omega_{R\tilde{K}})^2} \tag{42}$$

This expression will be used for our simulation of the experimental absorption spectrum, and it will also serve as the basis for our calculation of the fluorescence excitation spectra.

E. Calculation of Fluorescence Excitation Spectra. For the fluorescence excitation spectrum, we use a simple two-step-model: In the first step, the excited state $|\tilde{K}\rangle = |\tilde{E}, \tilde{k}\rangle$ is populated by absorption. In the second step, $|\tilde{K}\rangle$ fluoresces. The fluorescence excitation intensity $I_{\mathrm{fl}}(|\tilde{K}\rangle,\omega)$ is, accordingly, proportional to the population $P_{\mathrm{abs}}(|\tilde{K}\rangle,\omega)$ of level $|\tilde{K}\rangle$ due to absorption, times the probability $P_{\mathrm{fl}}(|\tilde{K}\rangle)$ of fluorescence,

$$I_{\mathrm{fl}}(|\tilde{K}\rangle,\omega) \propto P_{\mathrm{fl}}(|\tilde{K}\rangle) \cdot P_{\mathrm{abs}}(|\tilde{K}\rangle, \omega) \tag{43}$$

The population $P_{\mathrm{abs}}(|\tilde{K}\rangle, \omega)$ is, in the weak field limit, proportional to that contribution to the absorption coefficient $\alpha(\omega)$, which is due to the excitation of state $|\tilde{K}\rangle$. In the present model, where $\alpha(\omega)$ is a sum of Lorentzians (eq 42), we have that

$$P_{\mathrm{abs}}(|\tilde{K}\rangle,\omega) \propto A\omega \sum_R p_R \cdot |\mu_{R\tilde{K}}|^2 \cdot \frac{\Gamma_{\tilde{K}}}{(\Gamma_{\tilde{K}})^2 + (\omega - \omega_{R\tilde{K}})^2} \tag{44}$$

After excitation, $|\tilde{K}\rangle$ may decay either by IVR with rate $\Gamma_{\mathrm{IVR},\tilde{K}}$, eq 39, or by radiation with fluorescence decay rate $\Gamma_{\mathrm{rad},\tilde{K}}$, eq 40. Hence the probability of fluorescence decay is, in our model,

$$P_{\mathrm{fl}}(|\tilde{K}\rangle) = \frac{\Gamma_{\mathrm{rad},\tilde{K}}}{\Gamma_{\mathrm{rad},\tilde{K}} + \Gamma_{\mathrm{IVR},\tilde{K}}} = \frac{\Gamma_{\mathrm{rad},\tilde{K}}}{\Gamma_{\tilde{K}}} \tag{45}$$

Inserting eqs 44 and 45 into eq 43 yields

$$I_{\mathrm{fl}}(|\tilde{K}\rangle, \omega) \propto A\omega \sum_R p_R \cdot |\mu_{R\tilde{K}}|^2 \cdot \frac{\Gamma_{\mathrm{rad},\tilde{K}}}{(\Gamma_{\tilde{K}})^2 + (\omega - \omega_{R\tilde{K}})^2} \tag{46}$$

F. Results. At the given experimental temperature $T \approx 6$ K, the lowest doublet of torsional state $R = |0,0+\rangle$ and $R = |0,0-\rangle$ is populated almost exclusively and with almost equal probability. The Boltzmann populations of these initial states are therefore approximately given by

$$p_{0+}^0 = p_{0-}^0 \approx 1/2 \tag{47}$$

and $p_R = 0$ for all other states R.

Symmetry selection rules imply that any of the excited torsional states $|\tilde{K}\rangle$, which have either + or − symmetry, can be excited either from $R = |0,0+\rangle$ or $R = |0,0-\rangle$. As a consequence, eqs 42 and 46 for the absorption coefficient $\alpha(\omega)$ and the fluorescence excitation intensity $I_{\mathrm{fl}}(|\tilde{K}\rangle, \omega)$ simplify, i.e., the sum over the initial states $|R\rangle$ reduces to a single term, either $|0,0+\rangle$ or $|0,0-\rangle$.

In the following, we shall consider the special case when the absorption frequency ω is on resonance for the $|0,0+\rangle \rightarrow |\tilde{K}\rangle$ or $|0,0-\rangle \rightarrow |\tilde{K}\rangle$ transitions,

$$\omega = \omega_{\tilde{K}0\pm} \tag{48}$$

corresponding to the peak intensities of the relevant Lorentzians in expressions 42 and 46, thus

$$\alpha(\omega_{\tilde{K}0\pm}) = 0.5A\cdot\omega_{\tilde{K}0\pm}|\mu_{\tilde{K}0\pm}|^2\frac{1}{\Gamma_{\tilde{K}}} \quad (49)$$

for absorption, and

$$I_{\mathrm{fl}}(\tilde{K}, \omega_{\tilde{K}0\pm}) \propto 0.5\, A\cdot\omega_{\tilde{K}0\pm}|\mu_{\tilde{K}0\pm}|^2\frac{1}{\Gamma_{\tilde{K}}}\cdot\frac{\Gamma_{\mathrm{rad},\tilde{K}}}{\Gamma_{\tilde{K}}} \quad (50)$$

for the fluorescence excitation intensity. These results for the peak intensities in the low-temperature limit may be interpreted as follows: The absorption coefficient at the resonance frequency is proportional to the $\tilde{K}$, 0± dipole transition element squared; in the present approximation this is assumed to be proportional to the Franck−Condon coefficient squared,

$$|\mu_{\tilde{K}0\pm}|^2 \propto |\langle\tilde{K}|0\pm\rangle|^2 \quad (51)$$

Moreover, $\alpha(\omega_{\tilde{K}0\pm})$ is also reciprocal to the total relaxation rate $\Gamma_{\tilde{K}}$.

The fluorescence emission intensities have the same proportionalites to $|\mu_{\tilde{K}0\pm}|^2$ and $1/\Gamma_{\tilde{K}}$, but in addition there is another factor $\Gamma_{\mathrm{rad},\tilde{K}}/\Gamma_{\tilde{K}}$, in comparison with $\alpha(\omega_{\tilde{K}0\pm})$.

In the following, we shall adapt the experimental result, i.e., the radiative lifetimes $\tau_{\mathrm{rad},\tilde{K}}$ are nearly constant, $\tau_{\mathrm{rad},\tilde{K}} = \tau_{\mathrm{rad}} \approx$ 20 ns. Thus

$$\Gamma_{\mathrm{fl},\tilde{K}} \approx \frac{1}{\tau_{\mathrm{rad}}} = \mathrm{const} \quad (52)$$

As a consequence the ratios of

$$\frac{\alpha(\omega_{\tilde{K}0\pm})}{I_{\mathrm{fl}}(\tilde{K}, \omega_{\mathrm{fl}})} \propto \Gamma_{\tilde{K}} \quad (53)$$

and

$$\frac{|\mu_{\tilde{K}0\pm}|^2}{\alpha(\omega_{\tilde{K}0\pm})} \propto \Gamma_{\tilde{K}} \quad (54)$$

are both proportional to $\Gamma_{\tilde{K}}$.

The theoretical results (eqs 49−54) are illustrated in Figure 6. The top panel shows the Franck−Condon spectrum (eq 51); this is the hypothetical absorption spectrum of C9A which should be observed in the limiting case of zero couplings between the torsion and the other vibrations of C9A. Essentially, one should observe a spectrum with contributions from approximately 25 doublets of diabatic torsional states $|1k+\rangle$ and $|1k-\rangle$, from $k \approx 0$ to $k \approx 25$. The individual components of these doublets cannot be resolved with the available experimental resolution, due to their near degeneracies. The overall spectrum should have a pronounced peak near $k \approx 15$. This hypothetical case should serve as a reference, which is clearly different from the experimental absorption spectrum shown in Figure 5. In contrast with the top panel, the middle panel of Figure 6 shows the absorption spectrum according to the present model, eq 49. The comparison with the top panel shows two effects: (i) an overall shift of the Franck−Condon spectrum toward lower values of k and (ii) a depletion of the peak intensities close to the center of the absorption spectrum so that it appears to have (approximately) a rather broad plateau, extending from ca. $k = 8$ to $k = 17$, with small peaks close to $k = 10$ and $k = 15$. Comparison of eqs 49 and 51 shows that both effects (i) and (ii) are a consequence of the rates $\Gamma_{\tilde{K}}$ (41), see also eq 54. Indeed, in ref 26 it was shown that, in general, the $\Gamma_{\tilde{K}}$ increase with torsional quantum numbers, due to the increasing rates of IVR. This causes the first effect (i). Moreover, it was shown in ref 26 that the $\Gamma_{\tilde{K}}$ show an extraordinary increase close to $k \approx 12$, i.e., close to the crossing of the potential energy curves V^1 and V^2 of the diabatic bright and dark states (Figure 2). This crossing causes a rather strong coupling of S_2 and S_1 close to $k \approx 12$, and, as a consequence, a rather strong impact of the IVR in S_2. The net effect is, therefore, a substantial depletion of the absorption spectrum close to its center, as shown in the middle panel of Figure 6.

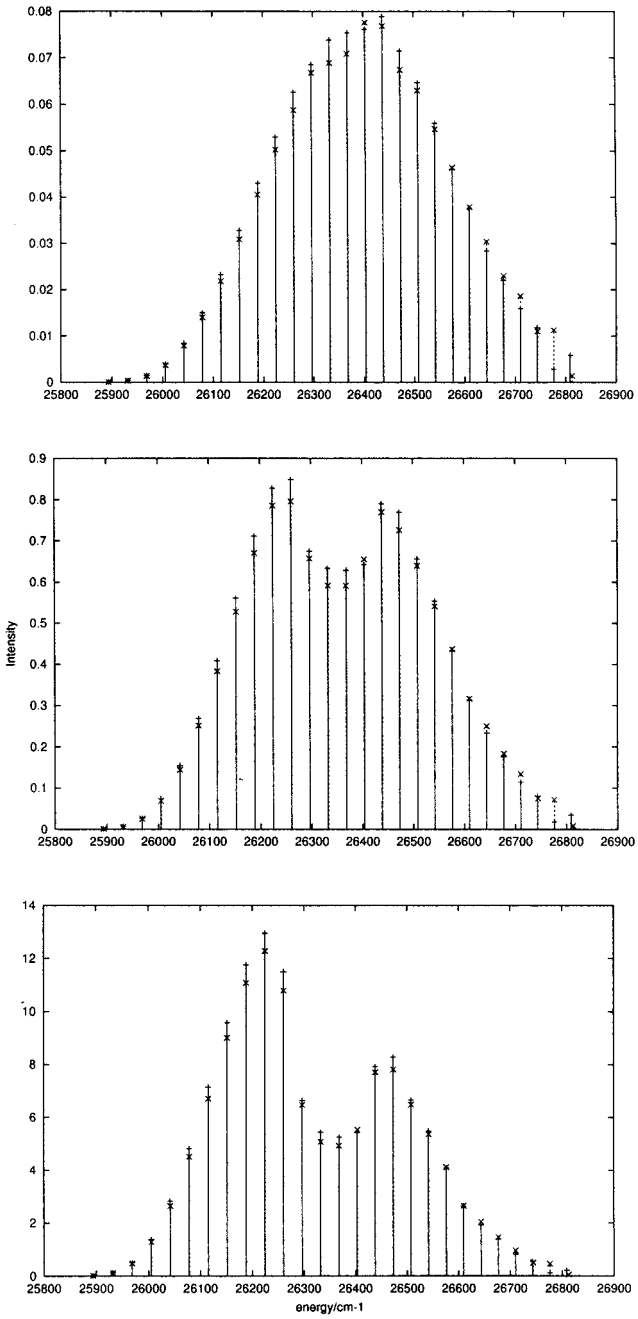

Figure 6. Simulated Franck−Condon (top panel), absorption (middle panel) and fluorescence excitation (bottom panel) spectra of C9A, calculated within our model, eqs 49−51 (see text). Transitions between levels with + and − symmetries are indicated by + and x, respectively.

Finally, the fluorescense excitation spectrum according to eq 50 is shown in the bottom panel of Figure 6. Comparison with the absorption spectrum shows the same effects (i) and (ii) as observed for the comparison of the absorption spectrum and the Franck−Condon spectrum, i.e., (i) an additional shift of the overall spectra toward lower values of k and (ii) an even deeper

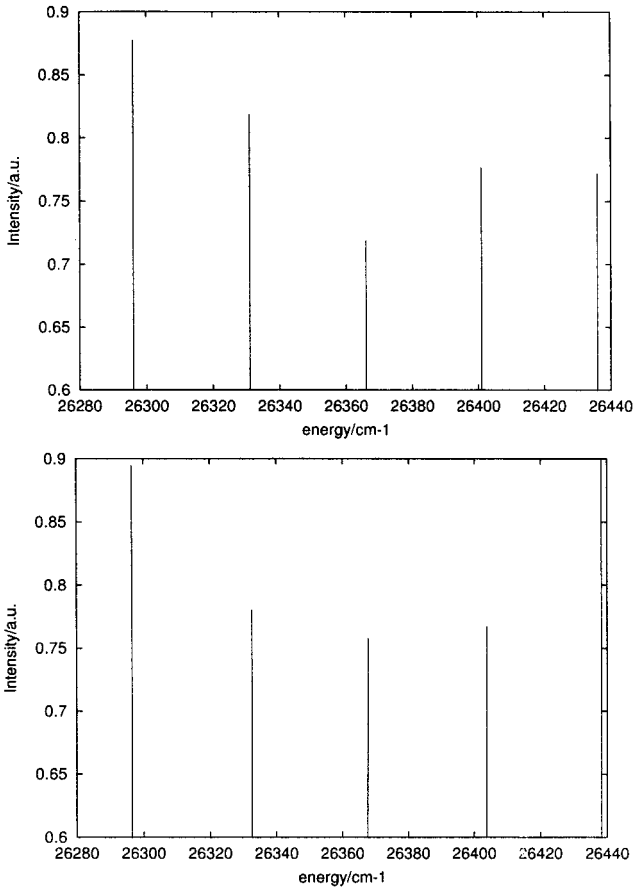

Figure 7. Comparison of selected bands (the same ones as in Figure 5) of the experimental (top panel) and simulated (bottom panel) absorption spectra. The transitions shown here correspond to the transitions given in Table 1.

'dip' in the spectrum close to $k \approx 12$, now causing an apparent double peak structure of the fluorescence excitation spectrum, with larger and smaller maxima close to $k = 9$ and $k = 16$, respectively. From eqs 53 and 54, it is obvious that it is again the behavior of $\Gamma_{\tilde{K}}$ that causes those effects, as discussed above.

The main trends of the theoretical spectra 6, i.e., a depletion of the intensities of the absorption spectra close to 26340 cm^{-1}, and an even stronger depletion of the fluorescence excitation spectrum agree, with the experimental trends (Figure 5), see also Figure 7. This confirms the simple model of ref 26 including an important detail, i.e., the much more rapid IVR in S_2 than in S_1. This result points to a much stronger coupling of the torsion to all other vibrations in S_2 than in S_1, and this in turn points to a different electronic structure of S_2 and S_1. This conjecture should be verified by a quantum chemical calculation.

IV. Quantum Chemical Calculations of the Adiabatic Electronic States

A. Computational Details. All Hartree−Fock-SCF (HF) and DFT calculations have been performed with the TURBOMOLE suite of programs.[42,43] Valence double-ζ Gaussian AO basis sets augmented with polarization functions on non-hydrogen atoms (VDZP, [3s2p1d]/[2s][44]) are used. Becke's hybrid exchange-correlation functional BHLYP[45] is employed in the DFT calculations. The geometries of C9A are taken from HF−SCF optimizations of the ground state using the VDZP AO basis. The torsional angle θ between the two aromatic units is taken as a reaction coordinate while optimizing all other geometric variables with the restriction of C_2 symmetry. All CI calculations are performed with an approximate resolution of the identity (RI) for the two-electron integrals.[46] The auxiliary basis sets used are taken from the TURBOMOLE library.[47] According to prior experience, the errors introduced by the RI method are less than 0.01 eV for the excitation energies and also the calculated properties are influenced very little. The DFT/MRCI calculations are performed as described in detail in ref 30. With an energy cutoff value of $0.9E_h$, about $1-1.5 \times 10^5$ configuration state functions (CSF) are selected for the three lowest states of A symmetry. The number of reference configurations varies between five and eight. The oscillator strengths (f) are calculated in the dipole-lengths form. The dipole moments are obtained as expectation values of the CI wave functions.

B. Results and Discussion. The optimized geometry of C9A in the ground state (S_0) at HF−SCF and DFT levels has C_{2v} symmetry with a perpendicular configuration of the two aromatic units, corresponding to $\theta = 90°$. The potential energy curve for the S_0 state is extremely flat (see Figure 8), in agreement with the experimental results. The double-minimum shape of the potential, however, could not be corroborated by the calculations. The tiny barrier of 17 cm^{-1} may result from a detailed balance between steric repulsion of the hydrogen atoms and dispersive interactions between the rings, which is out of the accuracy of current quantum chemical calculations for such a large molecule.

Before we discuss the properties of the excited states of C9A in detail, a qualitative discussion of the electronic structure seems appropriate here. Therefore, we plot the frontier molecular orbitals (MO) of C9A, which are most important in the CI wave functions of the excited states in Figure 9, for two twist angles.

At $\theta = 90°$, the MOs are strictly localized on the two aromatic subunits. The HOMO and LUMO correspond to the highest π and lowest π^* orbitals of anthracene, whereas the HOMO-1 is very similar to the HOMO of carbazole. In a simple one-electron picture, we expect two low-lying excited states: the first originates from the HOMO→LUMO single excitation ($21b_1 \rightarrow 22b_1$, see Figure 9) and is of A_1 symmetry in C_{2v} (L_a of anthracene using Platt's nomenclature[48]). The second is of charge-transfer (CT) type described by an excitation $22b_2 \rightarrow 22b_1$ (carbazole→anthracene) with A_2 symmetry. At $\theta = 90 \pm 20$ degrees, the symmetry is lower (C_2) and the HOMO and HOMO-1 mix strongly with each other. The HOMO-1 and HOMO then correspond to the bonding and antibonding linear-combinations of the anthracene and carbazole fragment MOs. It seems quite clear that for $\theta \neq 90°$, strong mixing of the former A_1 and A_2 states occurs so that the simple one-electron picture breaks down and only a CI calculation can provide accurate excited-state properties.

The potential energy curves along the twisting coordinate at the DFT/MRCI level are shown in Figure 8. Relative energies, dipole moments (μ), and oscillator strengths (f) are given in Table 2.

The S_1 state shows a symmetric double-minimum potential that is disturbed near $\theta = 90°$ due to the interaction with the CT state. The two minima are located at $\pm 25°$, which is in good agreement with the value of $\pm 26°$ deduced from experiment. Except near $\theta = 90$ degrees, this $2A_1$ state has little charge-transfer character. The dipole moment is 4.3 Debye at the minimum and decreases slightly to 1.5 D at $\theta = 90 \pm 2.5°$. The oscillator strength for the $S_0 \rightarrow S_1$ transition is quite large, with small variations between 0.16 and 0.22. The second excited state 3^1A is clearly of CT character. The dipole moment reaches values as large as 13.5 D, and the oscillator strength is <0.06. As expected, this state has a deep minimum at the perpendicular

TABLE 2: Results of DFT/MRCI Calculations for the Lowest Excited Adiabatic Singlet States of C9A[a]

	1^1A (S_0)		2^1A (S_1)			3^1A (S_2)		
θ	E	μ	E	μ	f	E	μ	f
90	0.0	1.91	28465.6	13.95	0.0	28816.4	2.05	0.208
87.5	7.9	1.90	28680.7	1.53	0.205	28990.8	13.51	0.005
85	47.8	1.89	28600.2	1.41	0.173	29221.7	10.54	0.038
80	114.3	1.87	28371.0	3.53	0.156	29590.7	8.32	0.057
70	344.8	1.77	28013.7	4.30	0.168	30366.7	7.28	0.054
65	551.8	1.70	27996.8	4.33	0.180	30882.3	7.02	0.049
60	917.9	1.61	28174.8	4.28	0.194	31583.1	6.86	0.043
50	2650.0	1.41	29191.0	3.97	0.222	33515.6	6.55	0.028

[a] Energies E (relative to the 1^1A state at $\theta = 90$ degree) are given in hc cm^{-1}, dipole moments μ in Debye.

twist angle of $\theta = 90$ degrees where the charge separation can be maximal. In a diabatic picture, the L_a and CT states cross near $\theta = 90$ degrees. At this point, the CT state is even lower in energy than the L_a state, which is clearly reflected by the drastic changes of the dipole moment and oscillator strengths. The crossing is, however, only weakly avoided due to the small electronic Hamiltonian matrix element between the singly excited L_a and CT configurations ($\langle L_a|\hat{H}_{\mathrm{el}}|\mathrm{CT}\rangle = 504$ cm^{-1} at $\theta = 90 \pm 2.5°$). These findings are in qualitative agreement with the experimental observations and definitely assign the dark state $S_2(S_X)$ to the CT state and confirm its energetic minimum for perpendicular twist angles, $\theta = 90$ degrees. The energtic position of the two potential energy curves with respect to each other is, however, in error by about 1000 cm^{-1} (0.12 eV, the CT state is calculated too high in energy), which is the typical error of the DFT/MRCI treatment for a molecule such as C9A with two states of totally different character. The error for the absolute excitation energy to the L_a state is about 2100 cm^{-1} (0.25 eV).

V. Conclusions

In this paper, experimental absorption and fluorescence excitation spectra of C9A in a supersonic jet expansion have been quantified and compared. At a certain excess energy, both types of spectra show irregularities, which can be modeled quantum chemically and quantum dynamically by a crossing of two excited states S_1 and S_2. These calculations are consistent with a lower lying S_1 state of locally excited character and small dipole moment, exhibiting a double minimum for the torsional coordinate. It is very weakly coupled to the background states. The S_2 state is of charge-transfer nature. It possesses an energetic minimum for perpendicular geometries, and its coupling is much larger leading to significant dissipation. The different behavior of S_1 and S_2 is consistent with the model of twisted intramolecular charge transfer (TICT) states and confirms the validity of the minimum overlap rule, even in this specific case of a large biaromatic system.

Acknowledgment. Support by the Deutsche Forschungsgmeinschaft (SfB 337), the Volkswagenstiftung (I/69642) and the Fonds der Chemischen Industrie is gratefully acknowledged. We should like to dedicate this paper to W. H. Miller.

Appendix

In this appendix, the analytical expression (eq 35) for the linear absorption coefficient $\alpha(\omega)$ is derived. To simplify the notation, the distinction between diabatic and adiabatic bases is not made, and a general system with system Hamiltonian $\hat{H}$ ($= \hat{H}_{\mathrm{tor}}$ in this paper) is considered, which supports two radiatively coupled, orthogonal electronic states. These system states are $|g\rangle$, the ground electronic state which supports (torsional: in general, internal nonelectronic) levels $|r\rangle$, $|s\rangle$, ..., whereas the electronically excited state $|e\rangle$ supports levels $|k\rangle$,$|l\rangle$, ...:

$$\hat{H}^{gg}|gr\rangle = E_r^g|gr\rangle \tag{A1}$$

$$\hat{H}^{ee}|ek\rangle = E_k^e|ek\rangle \tag{A2}$$

Our starting point for deriving eq 35 is the generalized Heller formula (eq 29). With the dipole operator given by

$$\hat{\mu} = \hat{\mu}^{eg}|e\rangle\langle g| + \mathrm{hc} \tag{A3}$$

and the initial, equilibrium density operator in excellent approximation given as

$$\hat{\rho}_0 = \hat{\rho}_0^{gg}|g\rangle\langle g| \tag{A4}$$

(where $\hat{\rho}_0^{gg} = e^{-\beta\hat{H}^{gg}}/\mathrm{tr}_g\{e^{-\beta\hat{H}^{gg}}\}$), one has

$$\hat{\sigma}_0 \equiv [\hat{\mu},\hat{\rho}_0] = \hat{\mu}^{eg}\hat{\rho}_0^{gg}|e\rangle\langle g| - \hat{\rho}_0^{gg}\hat{\mu}^{ge}|g\rangle\langle e| \tag{A5}$$

The operator $\hat{\sigma}(t) = e^{L\cup t}\hat{\sigma}$ evolves in time, with the initial condition (eq A5) according to

$$\frac{\partial\hat{\sigma}}{\partial t} = (L_H + L_D)\hat{\sigma} \tag{A6}$$

where (in the field-free case) for the Hamiltonian evolution,

$$L_H\hat{\sigma} \equiv -\frac{i}{\hbar}[\hat{H},\hat{\sigma}] = -\frac{i}{\hbar}[\hat{H}^{gg}|g\rangle\langle g| + \hat{H}^{ee}|e\rangle\langle e|,\hat{\sigma}] \tag{A7}$$

Electronic matrix elements of the Hamiltonian part are ($i, j = g, e$)

$$\frac{\partial\hat{\sigma}_H^{ij}}{\partial t} \equiv \langle i|L_H\hat{\sigma}|j\rangle = -\frac{i}{\hbar}(\hat{H}^{ii}\hat{\sigma}^{ij} - \hat{\sigma}^{ij}\hat{H}^{jj}) \tag{A8}$$

The dissipative term can generally be written as

$$L_D\hat{\sigma} = \sum_{i=g,ej=g,e}\sum |i\rangle\hat{\lambda}^{ij}\langle j| \tag{A9}$$

In the present case, dissipation is chosen to be of Lindblad[38] form (eq 23). Then

$$\hat{\lambda}^{ij} = \hat{C}^i\,\hat{\sigma}^{ij}\,\hat{C}^{j\dagger} - \frac{1}{2}\hat{C}^{i\dagger}\,\hat{C}^i\,\hat{\sigma}^{ij} - \frac{1}{2}\hat{\sigma}^{ij}\,\hat{C}^{j\dagger}\,\hat{C}^j \tag{A10}$$

where the $\hat{C}^i$ are Lindblad operators. According to the dissipation model for C9A introduced above, torsional dissipation takes place only in the excited state, and no electronic dissipation is accounted for. Hence, $\hat{C}^g = \hat{0}$ for the electronic ground state, and for the excited state, we have, in accord with eq 23

$$\hat{C}^e = \sum_{k=1}^{N_e}\sum_{l=1}^{N_e}\sqrt{\Gamma_{kl}^{ee}}|k\rangle\langle l| \tag{A11}$$

where Γ_{kl}^{ee} is the rate for the transition from level $|l\rangle$ in state $|e\rangle$, to $|k\rangle$ in the same state.

Electronic matrix elements of the dissipative part of the time evolution of $\hat{\sigma}$ are then

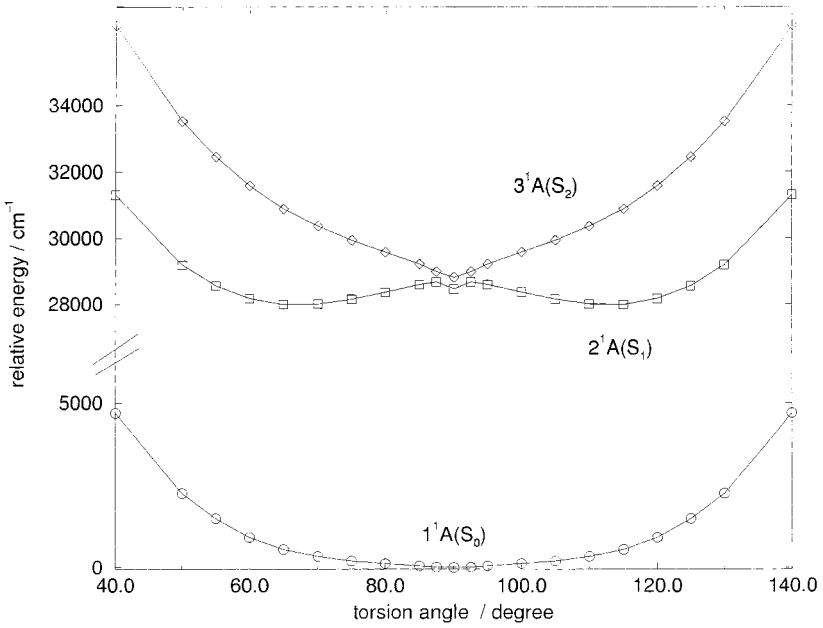

Figure 8. Potential energy curves (DFT/MRCI(VDZP)) for the three lowest singlet states of C9A, with avoided crossing of the CT and the DE state in the neighborhood of 90°.

$$\frac{\partial \hat{\sigma}_D^{\,gg}}{\partial t} \equiv \langle g|L_D\hat{\sigma}|g\rangle = 0 \tag{A12}$$

$$\frac{\partial \hat{\sigma}_D^{\,ge}}{\partial t} \equiv \langle g|L_D\hat{\sigma}|e\rangle = -\frac{1}{2}\hat{\sigma}^{ge}\,\hat{C}^{e\dagger}\,\hat{C}^{e} \tag{A13}$$

$$\frac{\partial \hat{\sigma}_D^{\,eg}}{\partial t} \equiv \langle e|L_D\hat{\sigma}|g\rangle = -\frac{1}{2}\hat{C}^{e\dagger}\,\hat{C}^{e}\,\hat{\sigma}^{eg} \tag{A14}$$

$$\frac{\partial \hat{\sigma}_D^{\,ee}}{\partial t} \equiv \langle e|L_D\hat{\sigma}|e\rangle = \hat{C}^{e}\,\hat{\sigma}^{ee}\,\hat{C}^{e\dagger} - \frac{1}{2}\hat{C}^{e\dagger}\,\hat{C}^{e}\,\hat{\sigma}^{ee} - \frac{1}{2}\hat{\sigma}^{ee}\,\hat{C}^{e\dagger}\,\hat{C}^{e} \tag{A15}$$

Before solving eqs A6−A15, it is first helpful to recall that for the absorption spectrum, according to eq 29, we have to evaluate the trace

$$\mathrm{tr}\{\hat{\mu}\,\hat{\sigma}(t)\} = \mathrm{tr}_g\{\hat{\mu}^{ge}\,\hat{\sigma}^{eg}(t)\} + \mathrm{tr}_e\{\hat{\mu}^{eg}\,\hat{\sigma}^{ge}(t)\} \tag{A16}$$

and Fourier transform it. Note that in eq A16, only the off-diagonal blocks of $\hat{\sigma}(t)$ show up. Because in the present case (field-free Hamiltonian, Lindblad dissipation) the electronic blocks of $\hat{\sigma}(t)$ remain uncoupled, it is possible to consider only the off-diagonal blocks and to evaluate eq A16 analytically.[28] To evaluate the individual traces in eq A16, we express all operators in a torsional state basis. Let N_g be the number of torsional eigenstates of the ground-state Hamiltonian $\hat{H}^{gg}$, which we use in a finite expansion, and N_e the analogous number of excited-state basis functions. Then,

$$\mathrm{tr}_g\{\hat{\mu}^{ge}\,\hat{\sigma}^{eg}(t)\} = \sum_{r=1}^{N_g}\langle r|\hat{\mu}^{ge}\,\hat{\sigma}^{eg}(t)|r\rangle = \sum_{r=1}^{N_g}\sum_{k=1}^{N_e}\mu_{rk}^{ge}\,\sigma_{kr}^{eg}(t) \tag{A17}$$

$$\mathrm{tr}_e\{\hat{\mu}^{eg}\,\hat{\sigma}^{ge}(t)\} = \sum_{k=1}^{N_e}\langle k|\hat{\mu}^{eg}\,\hat{\sigma}^{ge}(t)|k\rangle = \sum_{r=1}^{N_g}\sum_{k=1}^{N_e}\mu_{kr}^{eg}\,\sigma_{rk}^{ge}(t) \tag{A18}$$

where we used the notation

$$O_{rk}^{ge} \equiv \langle r|\hat{O}^{ge}|k\rangle = \langle gr|\hat{O}|ek\rangle \tag{A19}$$

for example. Now, the time evolution of the matrix elements in the off-diagonal block $\hat{\sigma}^{eg}$ of $\hat{\sigma}$ is given by

$$\frac{\partial \sigma_{kr}^{eg}}{\partial t} = \frac{\partial \sigma_{H,kr}^{eg}}{\partial t} + \frac{\partial \sigma_{D,kr}^{eg}}{\partial t} \tag{A20}$$

with

$$\frac{\partial \sigma_{H,kr}^{eg}}{\partial t} = -\frac{i}{\hbar}\sigma_{kr}^{eg}[E_k^e - E_r^g] \tag{A21}$$

$$\frac{\partial \sigma_{D,kr}^{eg}}{\partial t} = -\frac{1}{2}\langle k|\hat{\sigma}^{eg}\,\hat{C}^{e\dagger}\,\hat{C}^{e}|r\rangle \tag{A22}$$

where eqs A7 and A14 have been used. Using eq A22, we obtain,

$$\frac{\partial \sigma_{D,kr}^{eg}}{\partial t} = -\frac{1}{2}\sigma_{kr}^{eg}\sum_{l=1}^{N_e}\Gamma_{lk}^{ee} \tag{A23}$$

and

$$\frac{\partial \sigma_{kr}^{eg}}{\partial t} = \sigma_{kr}^{eg}\cdot a_{rk}^{eg} \tag{A24}$$

(with $a_{kr}^{eg} \equiv -{}^{i}/_{\hbar}[E_k^e - E_r^g] - {}^{1}/_{2}\sum_{l=1}^{N_e}\Gamma_{lk}^{ee}$). The last equation is solved by

$$\sigma_{kr}^{eg}(t) = \sigma_{0,kr}^{eg}\cdot\exp\{a_{kr}^{eg}\,t\} \tag{A25}$$

Because

$$\sigma_{0,kr}^{eg} = \mu_{kr}^{ge}\,p_r^g \tag{A26}$$

where

$$p_r^g = \mathrm{e}^{-\beta(E_r^g - E_0^g)}/Q \tag{A27}$$

is the Boltzmann weight of level r in the ground state at temperature $T = 1/(k_B\beta)$ (Q is again the torsional partition function), we have

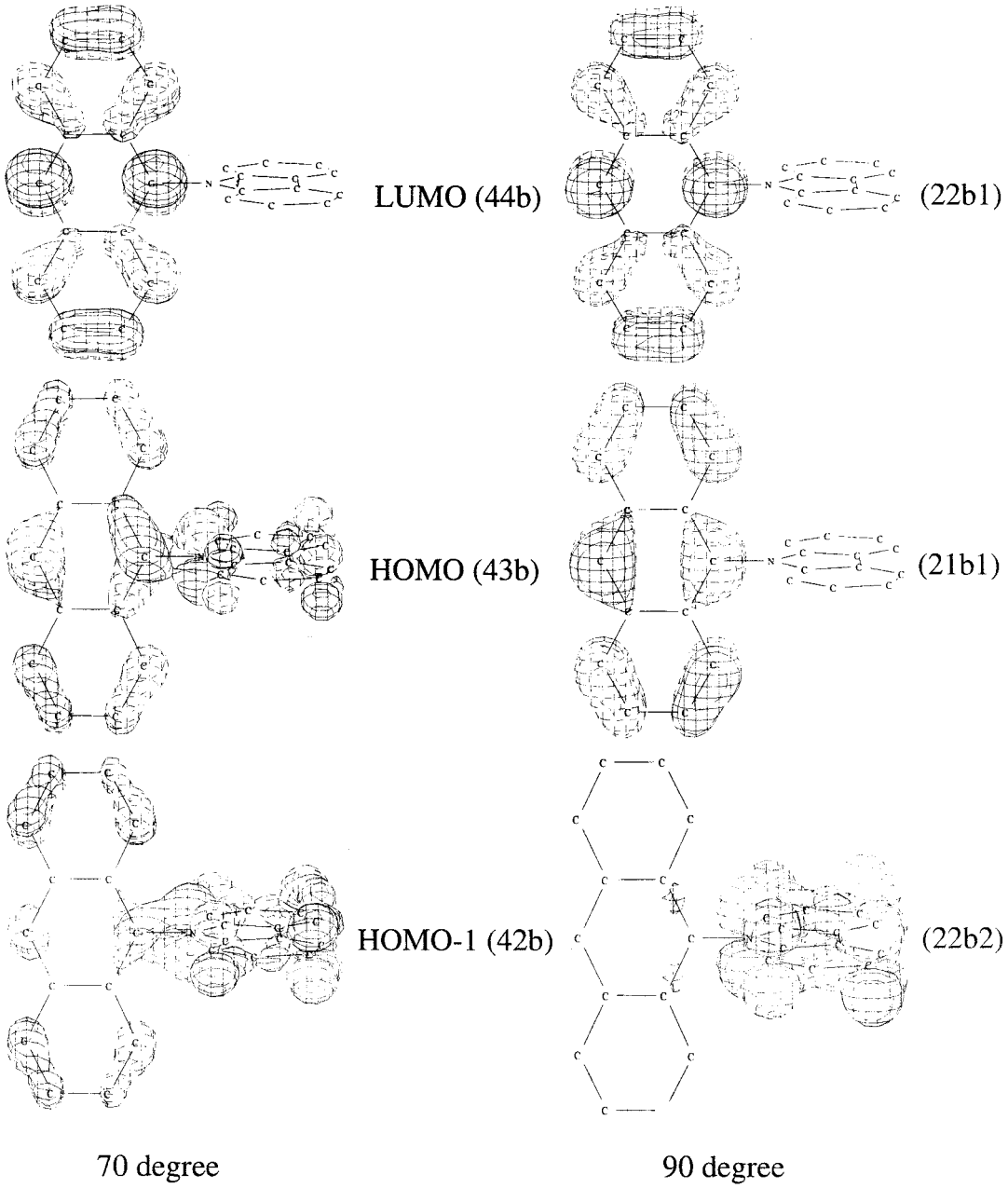

Figure 9. Frontier orbitals (DFT/BHLYP(VDZP)) of C9A for two torsional angles. The isosurfaces are drawn at a function value of 0.04 $a_0^{-3/2}$.

$$\sigma_{kr}^{eg}(t) = \mu_{kr}^{eg}\, p_r^g \cdot \exp\{a_{kr}^{eg}\, t\} \tag{A28}$$

An analogous derivation for the off-diagonal block $\hat{\sigma}^{ge}$ of $\hat{\sigma}$ yields

$$\sigma_{rk}^{ge}(t) = -\mu_{rk}^{ge}\, p_r^g \cdot \exp\{a_{kr}^{eg^*}\, t\} \tag{A29}$$

($a_{kr}^{eg^*}$ being the complex conjugate of a_{kr}^{eg}), and the total trace in eq A16 becomes

$$\mathrm{tr}\{\hat{\mu}\hat{\sigma}(t)\} = \sum_{r=1}^{N_g}\sum_{k=1}^{N_e} p_r^g |\mu_{kr}^{eg}|^2 \exp\left\{-\frac{1}{2}\sum_{l=1}^{N_e}\Gamma_{lk}^{ee} t\right\} \cdot 2i \sin\left(\frac{E_k^e - E_r^g}{\hbar} t\right) \tag{A30}$$

Finally, by using/defining[28] $E_k^e - E_r^g/\hbar = \omega_{kr}^{eg}$ and $\Gamma_{kk}^{ee} = \sum_{l\neq k}\Gamma_{lk}^{ee}$ one gets

$$\alpha(\omega) = A\omega \sum_{r=1}^{N_g}\sum_{k=1}^{N_e} p_r^g |\mu_{kr}^{eg}|^2 \,\mathrm{Re}\int_0^\infty \exp\{i\omega t\} \exp\{-\Gamma_{kk}^{ee} t\} \cdot 2i \sin(\omega_{kr}^{eg} t)\, \mathrm{d}t \tag{A31}$$

The integral can be done analytically;[28] when in the result antiresonances are neglected, the absorption coefficient becomes

$$\alpha(\omega) = A\omega \sum_{r=1}^{N_g}\sum_{k=1}^{N_e} p_r^g |\mu_{kr}^{eg}|^2 \frac{\Gamma_{kk}^{ee}}{\Gamma_{kk}^{ee2} + (\omega - \omega_{kr}^{eg})^2} \tag{A32}$$

Equation A32 is precisely the desired result (eq 35) when the appropriate adjustments for indices are made.

References and Notes

(1) Marcus, R. A. *J. Chem. Phys.* **1956**, *24*, 966.
(2) Marcus, R. A. *Annu. Rev. Phys. Chem.* **1964**, *15*, 155.

(3) May, V.; Kühn, O. *Charge and Energy Transfer Dynamics in Molecular Systems*, Wiley-VCH: Berlin, 2000.
(4) Grabowski, Z. R.; Rotkiewicz, K.; Siemiarczuk, A.; Cowley, D. J.; Baumann, W. *Nouv. J. Chim.* **1979**, *3*, 443.
(5) Rettig, W. *Angew. Chem.* **1986**, *98*, 969.
(6) Lippert, E.; Rettig, W.; Bonacic-Koutecky, V.; Heisel, F.;Miehé, J. A. *Adv. Chem. Phys.* **1987**, *68*, 1.
(7) Rettig, W. Electron Transfer I in *Topics in Current Chemistry*; Mattay, J., Ed.; Springer-Verlag, Berlin, 1994; Vol. 169, p 253.
(8) Marcus, R. A. *J. Phys. Chem.* **1989**, *93*, 3078.
(9) Herbich, J.; Kapturkiewicz, A. *Chem. Phys.* **1991**, *158*, 143.
(10) Herbich, J.; Kapturkiewicz, A. *Chem. Phys.* **1993**, *170*, 221.
(11) Herbich, J.; Kapturkiewicz, A. *Chem. Phys. Lett.* **1997**, *273*, 8.
(12) Kapturkiewicz, A.; Herbich, J.; Karpiuk, J.; Nowacki, J. *J. Phys. Chem.* **1997**, *101*, 2332.
(13) Herbich, J.; Kapturkiewicz, A. *J. Am. Chem. Soc.* **1998**, *120*, 1014.
(14) Maus, M.; Rettig, W.; Bonafoux, D.; Lapouyade, R. *J. Phys. Chem. A* **1999**, *103*, 3388.
(15) Schneider, F.; Lippert, E. *Ber. Bunsen-Ges. Phys. Chem.* **1968**, *73*, 1155.
(16) Rettig, W.; Zander, M. *Ber. Bunsen-Ges. Phys. Chem.* **1983**, *87*, 1143.
(17) Nakashima, N.; Murakawa, M.; Mataga, N. *Bull. Chem. Soc. Jpn.* **1976**, *49*, 854.
(18) Mataga, N.; Yao, H.; Okada, T.; Rettig, W. *J. Phys. Chem.* **1989**, *93*, 3383.
(19) Nagarajan, V.; Brearley, A. M.; Kang, T. J.; Barbara, P. F. *J. Chem. Phys.* **1987**, *86*, 3183.
(20) Barbara, P. F.; Kang, T. J.; Jarzeba, W.; Fonseca, T. In *Perspectives in Photosynthesis*; Jortner, J., Pullman, B., Eds.; Kluwer Academic Publishers: Dordrecht, 1990, *15*, 1.
(21) Kang, T. J.; Jarzeba, W.; Barbara, P. F.; Fonseca, T. *Chem. Phys.* **1990**, *149*, 81.
(22) Elich, K.; Kitazawa, M.; Okada, T.; Wortmann, R. *J. Phys. Chem. A* **1997**, *101*, 2010.
(23) Jurczok, M.; Plaza, P.; Martin, M. M.; Meyer, Y. H.; Rettig, W. *Chem. Phys.* **2000**, *253*, 339.
(24) Monte, Ch.; Roggan, A.; Subaric-Leitis, A.; Rettig, W.; Zimmermann, P. *J. Chem. Phys.* **1993**, *98*, 2580.
(25) Subaric-Leitis, A.; Monte, C.; Roggan, A.; Rettig, W.; Zimmermann, P.; Heinze, J. *J. Chem. Phys.* **1990**, *93*, 4543.
(26) Brackhagen, O.; Busse, H.; Giraud-Girard, J.; Manz, J.; Oppel, M. *J. Chem. Phys.* **2000**, *112*, 8819.
(27) Manz, J.; Proppe, B.; Schmidt, B. *Z. Phys. D* **1995**, *34*, 111.
(28) Scheurer, Ch.; Saalfrank, P. *J. Chem. Phys.* **1996**, *104*, 2869.
(29) Giraud-Girard, J.; Manz, J.; Scheurer, Ch. *Z. Phys. D* **1997**, *39*, 291.
(30) Grimme, S.; Waletzke, M. *J. Chem. Phys.* **1999**, *111*, 5645.
(31) O'Keefe, A.; Deacon, D. A. G. *Rev. Sci. Instrum.* **1988**, *59*, 2544.
(32) Boogarts, M. G. H.; Meijer, G. *J. Chem. Phys.* **1995**, *103*, 5269.
(33) Wheeler, M. D.; Newmann, S. M.; Orr-Ewing, A. J.; Ashfold, M. N. R. *J. Chem. Soc., Faraday Trans.* **1998**, *94*, 337.
(34) Zalicki, P.; Zare, R. N. *J. Chem. Phys.* **1995**, *102*, 2708.
(35) Lehmann, K. K.; Romanini, D. *J. Chem. Phys.* **1996**, *105*, 10263.
(36) Monte, C.; Rettig, W.; Zimmermann, P. *J. Chem. Phys.* in preparation.
(37) Monte, C.; Roggan, A.; Subaric-Leitis, A.; Rettig, W.; Zimmermann, P. *J. Chem. Phys.* **1993**, *98*, 2580.
(38) Lindblad, G. *Commun. Math. Phys.* **1976**, *48*, 119.
(39) Banin, U.; Bartana, A.; Ruhman, S.; Kosloff, R. *J. Chem. Phys.* **1994**, *101*, 8461.
(40) Neugebauer, F.; Malzahn, D.; May, V. *Chem. Phys.* **1995**, *201*, 151.
(41) Heller, E. J. *Acc. Chem. Res.* **1981**, *14*, 368.
(42) Ahlrichs, R.; Bär, M.; Häser, M.; Horn, H.; Kölmel, C. *Chem. Phys. Lett.* **1989**, *162*, 165.
(43) Treutler, O.; Ahlrichs, R. *J. Chem. Phys.* **1995**, *102*, 346.
(44) Schäfer, A.; Horn, H.; Ahlrichs, R. *J. Chem. Phys.* **1992**, *97*, 2571.
(45) Becke, A. D. *J. Chem. Phys.* **1993**, *98*, 1372.
(46) Weigend, F.; Häser, M. *Theor. Chem. Acc.* **1997**, *97*, 331.
(47) Weigend, F.; Häser, M.; Patzelt, H.; Ahlrichs, R. RI-MP2 optimized auxiliary basis sets available via anonymous ftp://ftp.chemie.uni-karlsruhe.de/pub/cbasen. *Chem. Phys. Lett.* **1998**, *294*, 143.
(48) Platt, J. R. *J. Chem. Phys.* **1949**, *17*, 484.